

Relationship between Morphological Change and Crystalline Phase Transitions of Polyethylene–Poly(ethylene Oxide) Diblock Copolymers, Revealed by the Temperature-dependent Synchrotron WAXD/SAXS and Infrared/Raman Spectral Measurements

Cao Weiyu,[†] Kohji Tashiro,^{*,†} Makoto Hanesaka,[†] Shinichi Takeda,[†] Hiroyasu Masunaga,[‡] Sono Sasaki,[‡] and Masaki Takata[‡]

Department of Future Industry-oriented Basic Science and Materials, Toyota Technological Institute, Tempaku, Nagoya 468-8511, Japan, and Japan Synchrotron Radiation Research Institute, Kouto, Sayo, Hyogo 679-5198, Japan

Received: October 19, 2008; Revised Manuscript Received: December 24, 2008

The phase transition behaviors of low-molecular-weight polyethylene–poly(ethylene oxide) (PE-*b*-PEO) diblock copolymers with the monomeric units of PE/PEO = 17/40 and 39/86 have been successfully investigated through the temperature-dependent measurements of wide-angle X-ray diffraction (WAXD), small-angle X-ray scattering (SAXS), infrared and Raman spectra, as well as thermal analysis. These diblock copolymers had been believed to show only order-to-disorder transition of lamellar morphology in a wide temperature region, but it has been found here for the first time that this copolymer clearly exhibits the three stages of transitions among lamella, gyroid, cylinder, and spherical phases in the heating and cooling processes. The WAXD and IR/Raman spectral measurements allowed us to relate these morphological changes to the microscopic changes in the aggregation states of PEO and PE segments. In the low-temperature region the PEO segments form the monoclinic crystal of (7/2) helical chain conformation and the PE segments of planar-zigzag form take the orthorhombic crystalline phase. These crystalline lamellae of PEO and PE segments are alternately stacked with the long period of 165 Å. In a higher temperature region, where the PEO crystalline parts are on the way of melting but the PE parts are still in the orthorhombic phase, the gyroid morphology is detected in the SAXS data. By heating further, the gyroid morphology changes to the hexagonally packed cylindrical morphology, where the orthorhombic phase of PE segments is gradually disordered because of thermally activated molecular motion and finally transforms to the pseudohexagonal or rotator phase. Once the PE segments are perfectly melted, the higher-order structure changes from the cylinder to the spherical morphology. These morphological transitions might relate to the thermally activated motions of two short chain segments of the diblock copolymer, although the details of the transition mechanism are unclear at the present stage.

Introduction

In a diblock copolymer the two different types of polymer segments tend to separate each other because of their immiscibility, but the existence of one covalent bond linking these two polymer segments controls the interfacial geometry and gives various kinds of morphologies as a result of microphase separation between these two polymer segments.¹ There have been synthesized various types of diblock copolymers that are important from both of industrial and scientific points of view. The two polymer components investigated for many years are mainly amorphous.² These amorphous–amorphous diblock copolymers are well-known to change their phase morphology among lamella, gyroid, cylinder, and sphere depending on temperature and/or the ratio of segmental lengths, but the molecular chains are of course in the amorphous state in all these phases. The combination of amorphous and crystalline components,³ or even that of crystalline and crystalline components,⁴ has been investigated in these years. In particular, the crystalline–crystalline diblock copolymers are scientifically

TABLE 1: Molecular Characteristics of PE-*b*-PEO Diblock Copolymers

notation	sample	Mn of PE ^a (g/mol)	Mn of PEO ^a (g/mol)	<i>M_w</i> / <i>M_n</i>
E17EO40	PE- <i>b</i> -PEO	500 (17)	1800 (40)	1.2
E39EO86	PE- <i>b</i> -PEO	1100 (39)	3800 (86)	1.1
<i>n</i> -C ₃₅ H ₇₂	<i>n</i> -alkane	492		1.0
PEO(43)	PEO		1900 (43)	1.1

^a The figures in parentheses indicate the averaged numbers of nonomeric units.

significant because they exhibit the various types of phase transitions and the drastic morphological changes in the crystallization process from the melt.⁴

Among the crystalline–crystalline diblock copolymers, polyethylene-*block*-poly(ethylene oxide) diblock copolymer (PE-*b*-PEO) is a typical combination of crystalline and crystalline components. This copolymer have become one of the most representative crystalline–crystalline diblock copolymers for the study of crystallization and phase transition behaviors because the two components have relatively simple chemical structures and much basic knowledge has been stocked in literature about the transition behaviors.^{5,6} For a long time this copolymer had

* To whom correspondence should be addressed. E-mail: ktashiro@toyota-ti.ac.jp.

[†] Toyota Technological Institute.

[‡] Japan Synchrotron Radiation Research Institute.

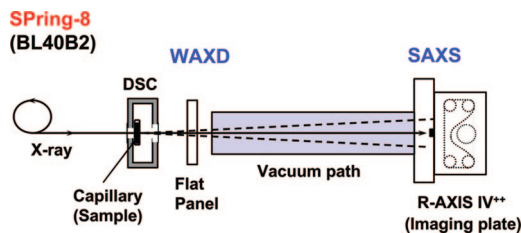


Figure 1. Schematic illustration of the simultaneous measurement system of 2D WAXD/SAXS patterns during the heating of sample set in the DSC cell.

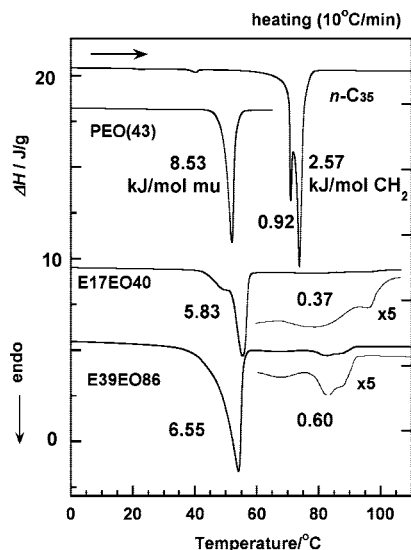


Figure 2. Themograms of E17EO40 and E39EO86 diblock copolymers in comparison with the corresponding *n*-alkane and pure PEO during heating process. The figures show the enthalpy changes in kJ/mol monomer unit.

been well-known as a surfactant of amphiphilic character, and it exhibits the various kinds of morphology such as cylinder, gyroid, and lamella depending on the concentration in an aqueous solution.^{1,7} The phase transitions of the neat PE-*b*-PEO system without any water component were not extensively reported.^{8–11} For example, Sun et al. studied the self-assembly and crystallization behavior of a low-molecular-weight PE-*b*-PEO copolymer with the molar ratio of 29/20 based on the wide-angle X-ray diffraction (WAXD) and infrared spectral data, and they proposed the morphology of alternately stacked lamellae consisting of individual components.^{8,9} When the sample was heated up, they reported that the stacked lamellar structure was still kept, but the chain packing disordering occurred in the lamellae. Castillo et al. reported the crystallization and melting behavior of PE-*b*-PEO diblock copolymers with E/EO = 82/18 and 89/11.¹⁰ These copolymers did not show, however, clear small-angle X-ray scattering (SAXS) peaks corresponding to the concrete morphology, but they were assigned to a distorted structure of spherical domains. As will be described in the present paper, we have investigated the phase transition behaviors of a series of the PE-*b*-PEO diblock copolymers with different PE/PEO ratios in a wide temperature range, and we have found clearly the existence of various kinds of morphologies such as gyroid, cylinder, and sphere in addition to the lamellar morphology by analyzing the SAXS data in detail. Of course, the different observation of the phase transition behavior between the present paper and the literature^{8–10} might come from the difference in the molar ratio and relative lengths of PE and PEO segments. In some cases the SAXS profiles are broad, making it difficult to detect small but significant peaks, which

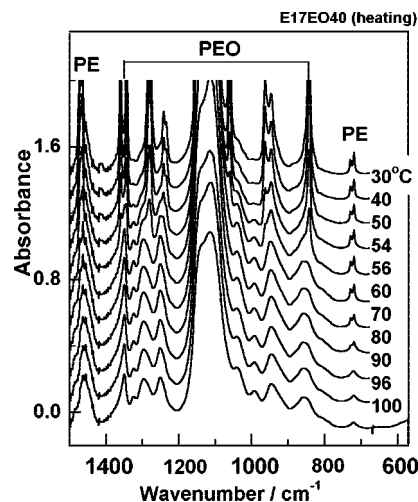


Figure 3. Temperature dependence of infrared spectra of E17EO40 in the frequency region of 1500–600 cm^{-1} measured in the heating process.

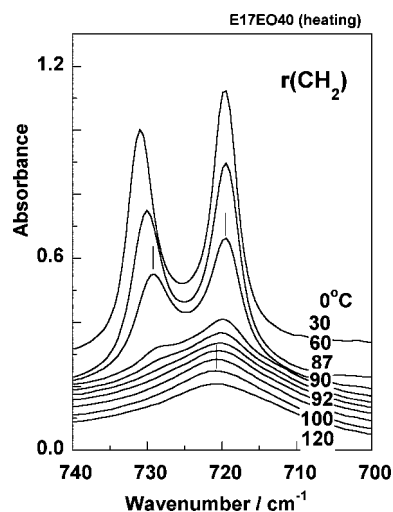


Figure 4. Temperature dependence of infrared spectra of E17EO40 in the frequency region of 740–700 cm^{-1} measured in the heating process.

are necessary for the identification of morphological characters. Our samples treated here show relatively clear SAXS peaks, allowing us to identify the morphologies of PE-*b*-PEO diblock copolymers concretely. Our new findings can be compared reasonably with the phase transition behavior of PE-*b*-PEO/water system as an ultimate state of no water content. Crystalline–amorphous diblock copolymer systems are also known to show the morphological transition between lamella, gyroid, and hexagonal cylinder phases; for example, poly(ethylene oxide)-*b*-polyethylethylene^{12,13} and poly(ethylene oxide)-*b*-poly(propylene oxide).^{14,15} The present PE-*b*-PEO diblock copolymer is a crystalline–crystalline diblock copolymer, but it changes to the crystalline–amorphous diblock copolymer once the PEO part is melted, since the PE part has higher melting point. In such a sense, the transitional behavior of PE-*b*-PEO diblock copolymer observed in the present work should be equivalent to that of amorphous–crystalline copolymers, as will be described in detail.

Another important point to be emphasized here is a success in the combination of the different types of techniques to determine the intimate relation between the structural changes at the molecular level and the morphological changes of mesoscopic scale. So far, the morphological study had been

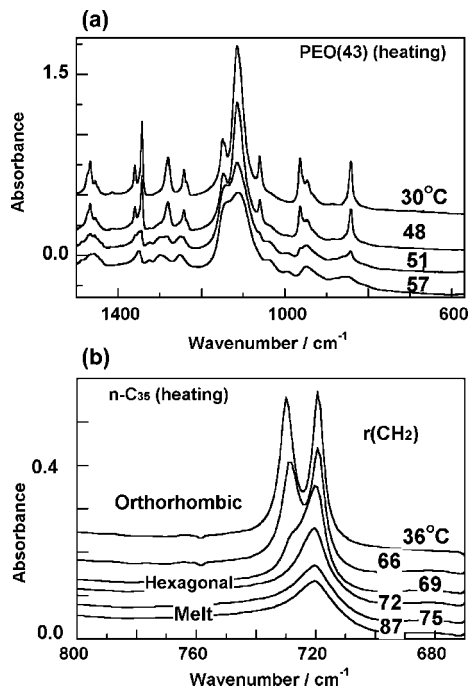


Figure 5. Temperature dependence of infrared spectra of (a) PEO (43) ($600\text{--}1500\text{ cm}^{-1}$) and (b) $n\text{-C}_{35}\text{H}_{72}$ ($670\text{--}800\text{ cm}^{-1}$) measured during the heating process.

made using the various techniques including SAXS, TEM, rheology, birefringence, and so on.¹⁶ An introduction of vibrational spectroscopic method may give us useful information about the relationship between the structural change viewed from the molecular level and the morphological change in a sub-micron scale by combining the IR/Raman spectral data with WAXD/SAXS data. In the present study, two types of PE-*b*-PEO samples with different chain lengths are used as the first trial to clarify the phase transitions in the heating process by means of simultaneous measurement of synchrotron SAXS and WAXD, the vibrational spectral measurement (IR/Raman), and differential scanning calorimetry (DSC).

Let us emphasize the novelty of our present work here. As mentioned above, the morphological changes among the lamella, gyroid, cylinder, and sphere are well-known phenomena for various types of diblock copolymers; amorphous–amorphous diblock copolymers and amorphous–crystalline diblock copolymers. Therefore, it might be naturally expected that we may observe the similar transition for the crystalline–crystalline PE–PEO diblock copolymer case. In fact, some researchers reported the transition behavior of this copolymer.^{8,9} Unfortunately they did not report the existence of gyroid, cylinder, and sphere morphologies. Of course, it might come from the difference in molecular weights of the samples, but we first need to report our new findings. Besides, the experimental clarification of the relationship between these morphological changes of nanometer-scale and the structural change in the molecular dimension has not been reported for many kinds of diblock copolymers. The organized combination of various kinds of techniques, in particular, the usage of infrared and Raman spectroscopic methods, has given us new information viewed from the molecular level, which was difficult to know from bulk properties such as rheology, birefringence, etc.

It is easily expected that the phase transition behaviors of these crystalline–crystalline diblock copolymers may be affected sensitively depending on the ratio of monomeric units of the two segments and the segmental lengths. In the present paper

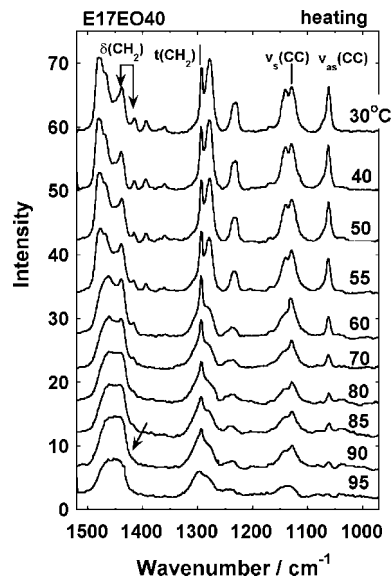


Figure 6. Temperature dependence of Raman spectra of E17EO40 measured during the heating process.

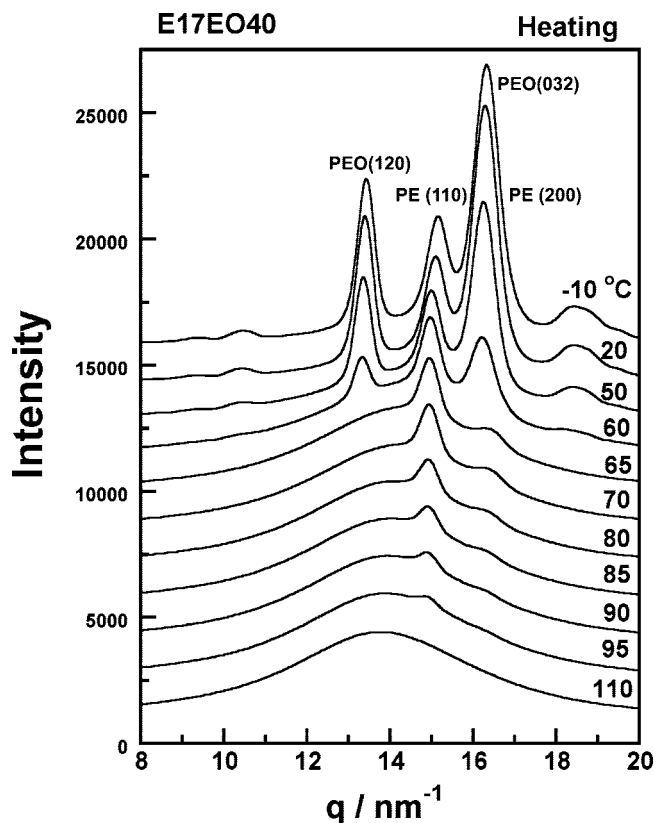


Figure 7. Temperature dependence of WAXD profile of E17EO40 measured in the heating process. The indices of main reflections are also shown here.

we will treat two types of PE-*b*-PEO diblock copolymer. A comparison of phase transition behavior between these two types of diblock copolymers is helpful for us to confirm the complicated phase transition phenomena, as will be discussed in this paper.

Experimental Section

a. Samples. The two members of PE-*b*-PEO diblock copolymers, E17EO40 and E39EO86, were purchased from

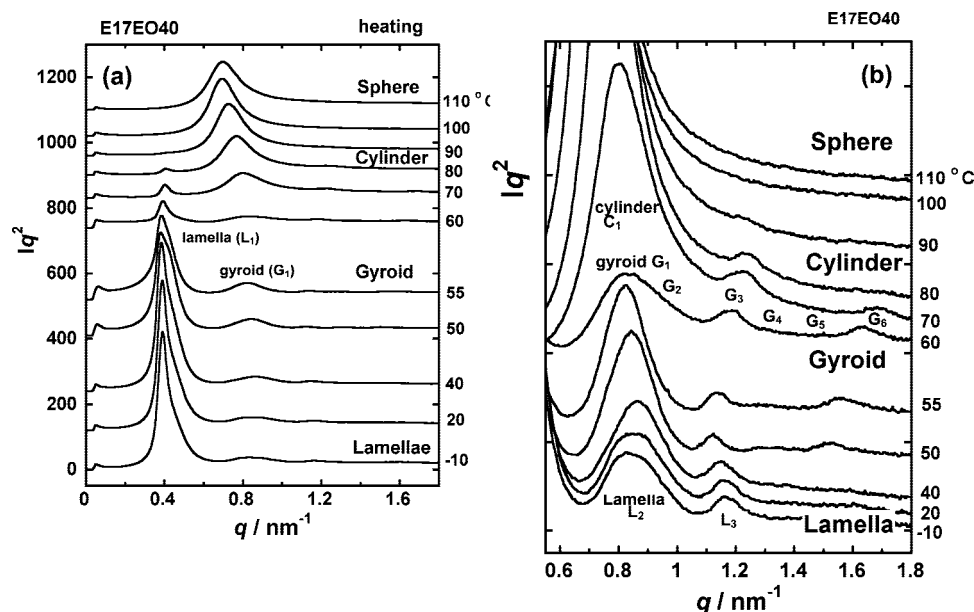


Figure 8. Temperature dependence of Lorentz-corrected SAXS profile of E17EO40 measured in the heating process: (a) $q = 0\text{--}1.8\text{ nm}^{-1}$ and (b) $q = 0.6\text{--}1.8\text{ nm}^{-1}$. The peak assignments are referred to in the text.

Polymer Source Inc. and possess the molecular characteristics shown in Table 1. These samples have almost monodispersed molecular weights. For comparison, *n*-alkane and PEO with almost the same chain lengths as those of E17EO40 were also investigated.

The samples were heated to 120 °C, above the melting points of pure PE (*n*-alkane) and PEO components, and then slowly cooled to room temperature. The thus-obtained samples were supplied to the measurements.

b. Measurements. Raman spectra were measured with a Japan Spectroscopic Company NRS-2100 laser Raman spectrophotometer at the back-scattering geometry using the 532 nm line as an excitation beam. The temperature-dependent measurements of Raman spectra were performed at constant temperatures during the heating process using a Linkam optical microscope heater (10036).

Infrared spectral measurements were performed using a Varian FTS7000 Fourier-transform infrared spectrometer. The infrared spectra were taken at a resolution power of 1 cm^{-1} . KBr disks were prepared, which were melted and cooled to an ambient temperature to supply to the measurement.

The simultaneous measurements of 2D-WAXD and SAXS data were performed at the BL40B2 beam line at SPring-8 (Japan Synchrotron Radiation Research Institute, Hyogo, Japan). The wavelength of the incident X-ray beam was 1.00 \AA . A Rigaku R-Axis IV⁺⁺ imaging plate system and a Hamamatsu flat panel were used, respectively, as the 2D detectors for SAXS and WAXD measurements. The samples were put into capillaries and sealed off. They were melted and then cooled down to room temperature to eliminate the air bubbles. The capillary was packed into an aluminum pan, which was set to the DSC cell (Metlar Toledo FP90). The X-ray exposure time was 2 and 4 s, respectively, for taking a set of WAXD and SAXS data at the heating rate of 10 °C/min . The schematic illustration of the whole system is given in Figure 1.

The thermal behaviors of the samples were investigated using a TA Instruments DSC Q1000 under nitrogen gas atmosphere at a heating rate of 10 °C/min .

Results and Discussion

a. Thermal Analysis. Figure 2 shows the DSC thermograms measured for E17EO40 and E39EO86 diblock copolymers in the heating process as well as those of *n*-alkane (*n*-C₃₅H₇₂) and pure PEO. The relatively sharp endothermic peak at around 55 °C corresponds to the melting point of the PEO component. The melting point of the PEO component is a slightly shifted toward the lower temperature side for the E39EO86 sample, but the essential feature is the same as that of E17EO40. In the higher temperature region there are several broad peaks overlapped, which are considered to include the phase transition from orthorhombic to hexagonal phase of the PE component. The detailed assignment can be made as described in a later section. The total enthalpy change in these temperature regions is about 0.37 kJ/mol CH_2 unit (E17EO40) and 0.60 kJ/mol CH_2 unit (E39EO86), which are much smaller than those detected for the ortho-to-hexagonal (0.92) and hexagonal-to-melt transition (2.57) of *n*-C₃₅H₇₂.

b. Infrared Spectral Changes. The temperature dependence of infrared spectra of E17EO40 diblock copolymer measured in the heating process is shown in Figures 3 and 4 in the frequency regions of $1500\text{--}600\text{ cm}^{-1}$ and $740\text{--}700\text{ cm}^{-1}$, respectively. By comparing with the spectra of the corresponding *n*-alkane and PEO (Figure 5), a pair of bands at 719 and 730 cm^{-1} is known to come from the correlation splitting of an orthorhombic unit cell of the PE crystal.^{17,18} The splitting width became smaller with an increase in temperature and changed to a singlet at 721 cm^{-1} . This band is characteristic of the pseudohexagonal phase or rotator phase of *n*-alkane (see Figure 5b).^{19–22} It decreased in intensity with increasing temperature and changed to the band of the melt. In this way the orthorhombic phase of PE segments is gradually disordered in packing mode and transforms to the rotator phase before the melting. The other infrared bands observed in the $1500\text{--}700\text{ cm}^{-1}$ region come from the monoclinic crystal of PEO chains with $(7/2)$ helical conformation.⁶ By increasing the temperature, as seen in Figures 3 and 5, these crystalline bands of the PEO component became weaker and disappeared at about 55 °C, corresponding to the melting point of PEO crystal and being

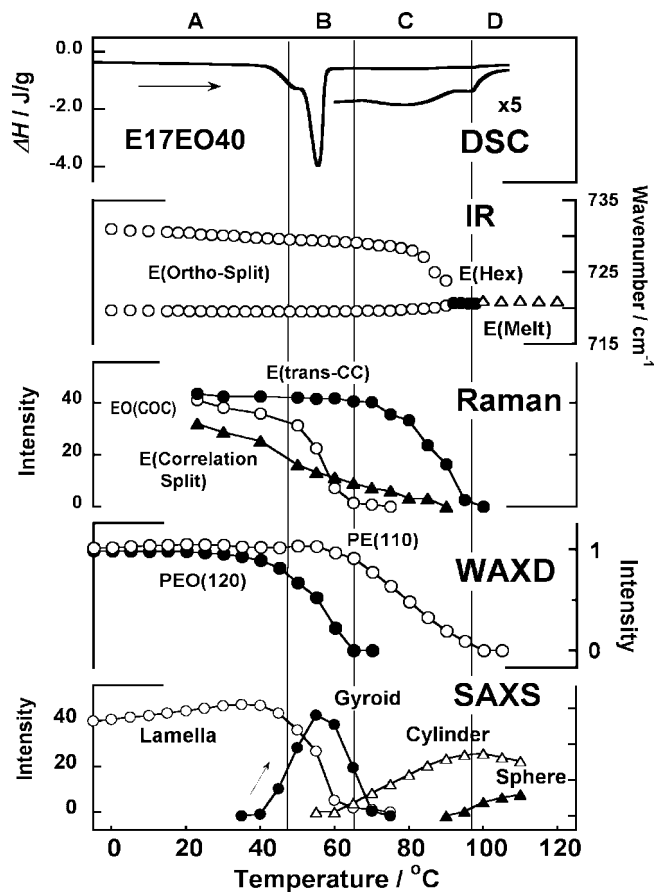


Figure 9. Correlation of the DSC, IR, Raman, WAXD, and SAXS data collected for E17EO40 in the heating process.

consistent with the DSC result. In the $2800\text{--}3000\text{ cm}^{-1}$ region of CH_2 stretching modes (not shown here) a new band started to appear as a shoulder of antisymmetric CH_2 stretching band [$\nu_{\text{as}}(\text{CH}_2)$]. This observation is compared with the spectral change detected for pure *n*-alkane, corresponding to the generation of gauche bonds in the C—C skeletal chains.^{19–22} Therefore, it may be said that the PE segments in the diblock copolymer show the phase transition from the orthorhombic phase of all-trans zigzag chains to the conformationally disordered pseudo-hexagonal phase in the temperature region of $80\text{--}90\text{ }^\circ\text{C}$. The band corresponding to the $\text{OH}\cdots\text{O}$ hydrogen bond of solid-state PEO segments is detected at 3450 cm^{-1} , indicating the end groups of PEO segments belonging to the neighboring chains are connected to each other. The peak position shifts to the higher wavenumber side, reflecting a decrease in hydrogen bond strength in the molten state above $60\text{ }^\circ\text{C}$. The similar infrared spectral changes are also observed for E39EO86 diblock copolymer.

The transition from orthorhombic to hexagonal phase in the PE segmental part can be observed more clearly in the Raman spectra shown in Figure 6. For example, a pair of the $\delta(\text{CH}_2)$ bands at 1416 and 1438 cm^{-1} come from the correlation splitting.^{17,18} As the temperature was increased, the intensity of one component at 1416 cm^{-1} decreased and disappeared at about $90\text{ }^\circ\text{C}$, indicating the transition to the pseudo-hexagonal phase.^{19–22} The stretching modes of skeletal C—C bonds at 1130 cm^{-1} [$\nu_{\text{s}}(\text{CC})$] and 1060 cm^{-1} [$\nu_{\text{as}}(\text{CC})$] and the CH_2 twisting band at 1295 cm^{-1} [$\tau(\text{CH}_2)$] were observed even in this temperature region, indicating that the zigzag chain segments still remained, although the relative intensities were lower due to the partial disordering in the conformation. As a result, these chain segments lose their

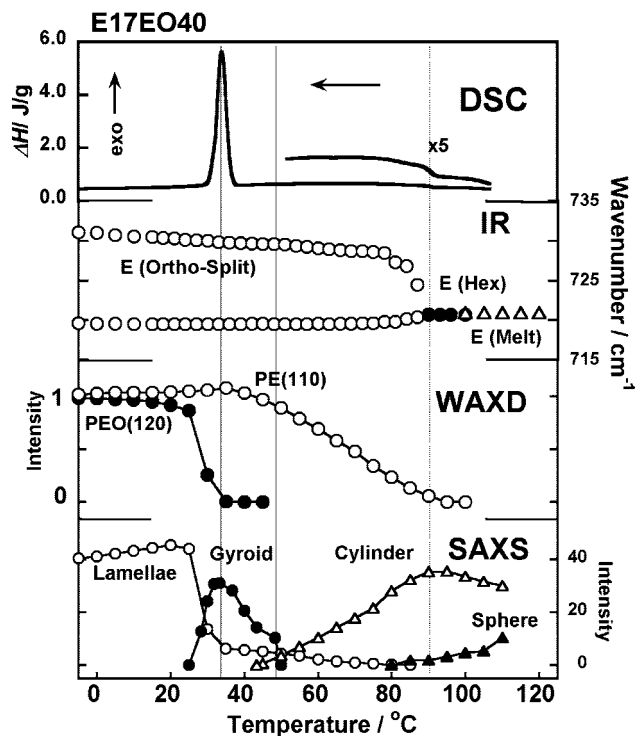


Figure 10. Correlation of the DSC, IR, Raman, WAXD, and SAXS data collected for E17EO40 in the cooling process.

motional correlation as the temperature increases to approach the rotator phase. Different from the rotator phase of *n*-alkane,^{23–26} however, the PE segments of the diblock copolymer is not considered to rotate freely, but it experiences the librational motion of a limited amplitude. In a higher temperature region the PE parts are perfectly melted as known from the disappearance of Raman and infrared bands characteristic of planar-zigzag conformation.

c. Temperature Dependence of WAXD and SAXS. The 2D SAXS/WAXD patterns were measured for E17EO40 in the heating process using a synchrotron X-ray system, from which the 1D scattering profiles were obtained as shown in Figures 7 and 8. As seen in Figure 7, the WAXS profiles at low temperatures are the overlap of those of PE and PEO crystals. At ca. $60\text{ }^\circ\text{C}$ the PEO peaks disappeared due to the melting. In the temperature region of the pseudo-hexagonal phase of PE segments, the corresponding reflections were difficult to detect clearly because of the overlap of the strong halo profile coming from the melt of the PEO component, although the infrared and Raman spectra clearly indicate the presence of the pseudo-hexagonal phase as already described in the preceding section. As shown in Figure 8, panels a and b, the SAXS profile was found to change remarkably with temperature. At room temperature the peaks are broad, but the ratio of the peak positions is $L_1:L_2:L_3\cdots = 1:2:3:4$, indicating an existence of stacked lamellar structure. The long period of the stacked lamellae is $165\text{ }\text{\AA}$. The SAXS pattern changed remarkably upon heating. In the region of $50\text{--}60\text{ }^\circ\text{C}$, the peaks became sharper, and the peak positions were detected at $G_1:G_2\cdots G_6 = 1:1.15:1.53:1.63:(1.83):2$. This ratio is typical of the gyroid structure.^{1,27}

Figure 9 compares all the data collected for IR, Raman, WAXD, and SAXS measurements. In the temperature region where the gyroid pattern is observed, the PEO segments are in the melting state and the PE segments are still in the crystalline state of orthorhombic phase. As the temperature is increased further, the SAXS pattern typical of hexagonally packed

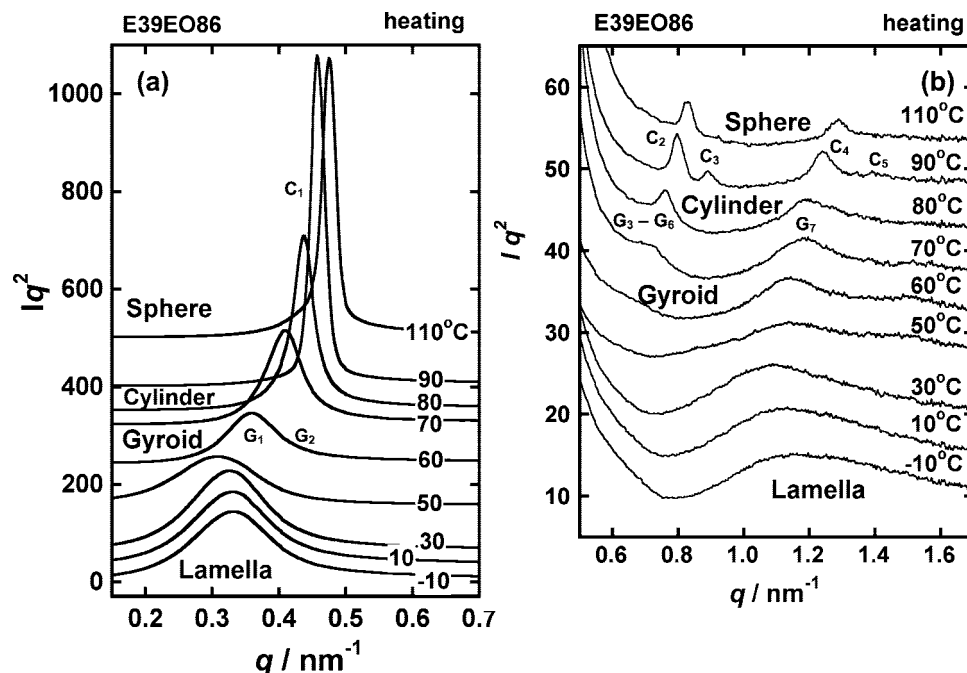


Figure 11. Temperature dependence of SAXS profile of E39EO86 measured during the heating process: (a) $q = 0.1\text{--}0.7\text{ nm}^{-1}$ and (b) $q = 0.5\text{--}1.7\text{ nm}^{-1}$. The peak assignments are referred to in the text.

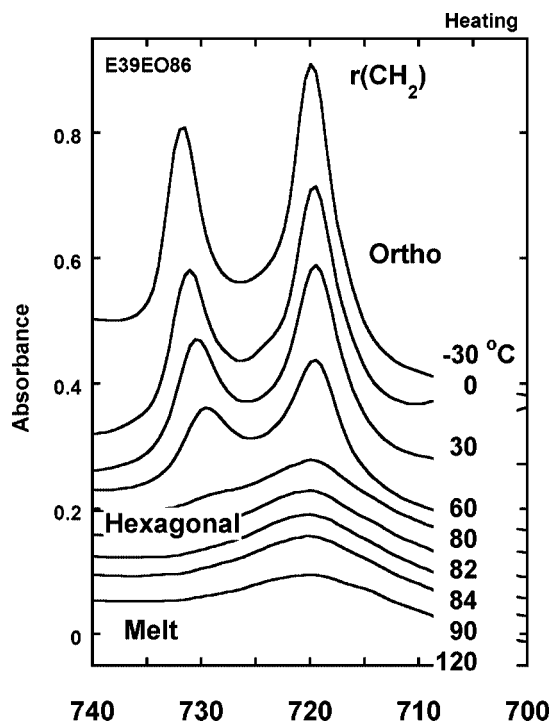


Figure 12. Temperature dependence of infrared spectra of E39EO86 in the frequency region of $740\text{--}700\text{ cm}^{-1}$ measured in the heating process.

cylindrical phase is detected, as seen in Figure 8; the ratio of peak positions is 1:1.73:2:2.65:3. The IR and Raman data tell us that the PE segments started to disorder and gradually transferred to the rotator phase in this temperature region. As the temperature was further increased to about $100\text{ }^{\circ}\text{C}$, the signals of the rotator phase disappeared, the PE segments changed to the molten state perfectly, and the cylindrical phase transformed to the disordered spherical phase. The transition behavior is reversible and the transition from sphere to cylinder, gyroid, and to lamellae is observed as shown in Figure 10, where

the various experimental data collected in the cooling process are compared.

The similar but clearer observation was made for the case of E39EO86 copolymer, as shown in Figure 11. At low temperature, the SAXS peaks are detected at the positions of the ratios 1:2:3:4, indicating the stacked lamellar structure. Around $60\text{--}70\text{ }^{\circ}\text{C}$, where the PEO segments are almost melted and the PE segments are still in the orthorhombic phase, the positions of the observed SAXS peaks may be assigned to those predicted for the gyroid phase, although the peaks are broad and many peaks are considered to overlap as seen in Figure 11 ($G_1\text{:}G_2\text{:}G_3\text{:}G_4\text{:}G_5\text{:}G_6\text{:}G_7 = 1\text{:}1.15\text{:}1.53\text{:}1.63\text{:}1.83\text{:}1.91\text{:}2.88$). In a higher temperature region of ca. $80\text{ }^{\circ}\text{C}$, the orthorhombic phase of PE transforms to the rotator phase, as determined from the IR spectra given in Figure 12, just when the cylindrical phase is detected in the SAXS data ($C_1\text{:}C_2\text{:}C_3\text{:}C_4\text{:}C_5 = 1\text{:}1.73\text{:}2\text{:}2.65\text{:}3$). Above $95\text{ }^{\circ}\text{C}$ the peak intensities of the cylindrical phase decrease gradually, and this phase transforms to the spherical phase. All of the IR, WAXD, and SAXS data are compared in Figure 13. It should be noticed here that the two phases coexist during the transition processes, suggesting the transitions occur in the thermodynamic first-order modes for both of these two copolymers. The transitions occur reversibly in both the heating and cooling processes.

d. Structural Changes Viewed from Various Levels. In this way, both of E17EO40 and E39EO86 copolymers exhibit essentially the same phase transition behavior with each other. Figure 14 shows the correspondence in the structural changes viewed by the WAXD, IR, Raman, and SAXS data. The lamellar structure is realized when both the PE and PEO segmental parts exist as the crystalline states. Once the PEO crystalline phase starts to melt, or is being melted but the PE crystalline phase is still existent as the orthorhombic state, the lamellar morphology starts to transform to the gyroid morphology. In a higher temperature region the PE orthorhombic phase is gradually disordered and transforms to the pseudohexagonal or rotator phase, where the hexagonally packed cylindrical morphology is formed on a larger scale. Once both PE and PEO segments

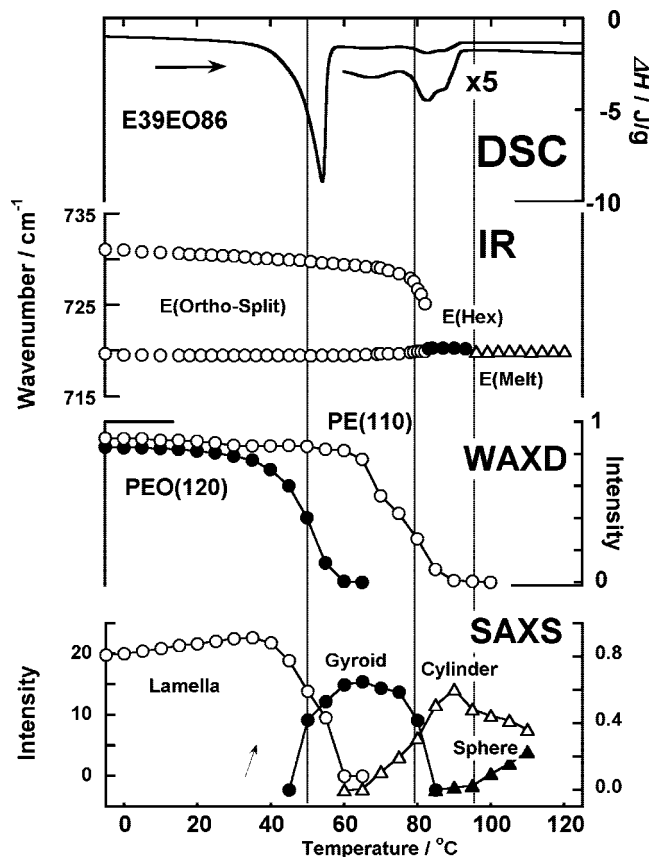


Figure 13. Correlation of the DSC, IR, WAXD, and SAXS data collected for E39EO86 in the heating process.

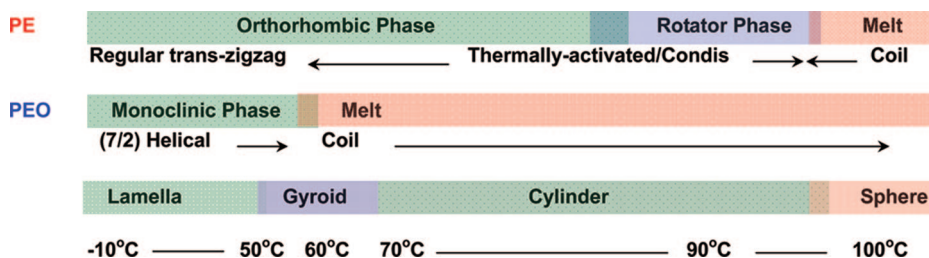


Figure 14. Comparison of structural changes of PE-*b*-PEO diblock copolymers viewed from the various levels. The temperature regions shown here are for the case of E17EO40 copolymer.

are perfectly melted, the cylindrical morphology disappears and the disordered state or spherical morphology appears. These phase transitions correspond to the several overlapped and broad peaks observed in the DSC thermograms.

Figure 15 shows a schematic illustration of the relationship between the molecular and crystal structural transition and the morphological change in the mesoscopic scale. In the low-temperature lamellar structure, the PEO segments are arranged face-to-face to form the intermolecular hydrogen bonds, and the PE segments are similarly packed so that the methyl groups are in contact with each other. Because the connection parts of trans-zigzag PE and helical PEO segments are not geometrically well-matched, the interlamellar parts between these two segments might be more-or-less disordered. As a result, the repeated period of the stacked lamellae consisting of ordered and disordered structural parts is 165 Å at room temperature. This structural model may be reasonable by taking into account the low degree of crystallinity as estimated from the DSC data. At present it is not clear whether or not the PE or PEO segmental parts are tilted to the normal of lamellar surfaces, so the tilted structure is now out of consideration in Figure 15. Once the PEO segments change from regular (7/2) helical conformation

to the more disordered chain form, the stacked lamellar structure changes to the gyroid, where it is not clear at present whether the lamellar structure transforms temporarily to the disorder phase such as a perforated layer structure or not.^{8,9} A similar situation is observed when the PE segments are conformationally disordered and lose the motional correlation between the neighboring chain stems, where the gyroid structure transforms immediately to the cylindrical morphology. It continues to exist until the parallel packing of PE stems is kept even though the chain conformation is disordered below the melting point.

It is difficult at the present stage to draw the concrete and definite transition mechanism of PE-*b*-PEO copolymer from the data presented here only. One of the most difficult and interesting phenomena is that the PE segmental parts are still in the orthorhombic phase even when the lamellar structure disappears due to the melting of PEO crystal region and the gyroid morphology starts to appear. Another point is that the gyroid-to-cylinder transformation occurs when the correlation of two chain segments in the orthorhombic cell, as represented by the splitting width of $r(\text{CH}_2)$ bands, starts to decrease and the trans conformation starts to disorder at around 60–70 °C. After that, the relative amount of gyroid starts to decrease and

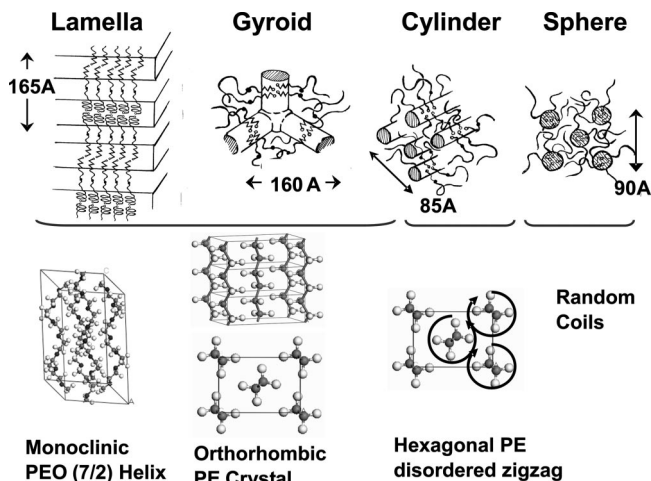


Figure 15. Schematic illustration of structural changes of PE-*b*-PEO diblock copolymers viewed from the various levels.

the cylinder phase increases its relative amount. The peak of the cylinder phase is observed when the orthorhombic-to-rotator phase transition occurs in the PE segmental parts (about 90–100 °C). These tendencies can be detected for both the two diblock copolymers, although the temperature regions of the existence of these phases are different between these two samples. By comparing the inner structural change and the morphological change, we may consider that an increase in the thermal mobility of PEO and PE segments causes these remarkable changes in morphology. The orthorhombic packing mode of PE segmental parts does not necessarily mean the rigid and tight packing of molecular chains. For example, pentadecanoic acid is known to show the orthorhombic-to-orthorhombic packing mode change in a relatively narrow temperature region of 46 °C: the zigzag chain segments experience the flip-flop motion to change their orientation direction between the *a* and *b* axes (refer to Figure 15).²⁹ In this transition, the splitting of infrared bands intrinsic to the orthorhombic packing mode is kept, but the molecular chains experience remarkable cooperative flip-flop rotational motion around the chain axis. In the present case both the PEO and PE segments are short, and the segmental motions start to occur relatively easily. Therefore, as a possibility, the PE segments of PE-*b*-PEO diblock copolymer might experience such a cooperative flip-flop-type rotational motion around the chain axis in the lamella-to-gyroid morphological transition where PEO segments are already thermally activated, and as a result the copolymer chains might move relatively easily their positions as a whole to form the gyroid structure. More drastic thermal motion in the PE segmental parts might cause the morphological change from gyroid to cylinder and even to sphere.

Anyhow, it is still difficult to describe the true transition mechanism observed for PE-*b*-PEO diblock copolymer with relatively short chain segments. The solid-state NMR spectral measurement might give us useful information about the molecular motion of the PE segments as a function of temperature. Molecular dynamics calculation is also useful for the discussion of molecular mobility in the diblock copolymer. It should be noticed here that the lamella–gyroid–cylinder–sphere morphological transition seems to occur apparently without any clear correlation with the inner structural changes of PE and PEO segments. We need to find a key factor as a trigger for these complicated phase transition phenomena of PE-*b*-PEO diblock copolymers in future.

Conclusions

In the present paper we have reported the complicated phase transition behaviors of PE-*b*-PEO diblock copolymers E17EO40 and E39EO86 viewed from various levels on the basis of infrared and Raman spectra and WAXD and SAXS data. The crystalline lamellae of PE and PEO are alternately stacked at low temperature. Once the PEO components start to melt, the lamellar structure changes to the gyroid structure, where the PE segments are still in the orthorhombic crystalline phase. In the process of the structural disordering in the orthorhombic phase of the PE part and the transition to the pseudohexagonal phase or rotator phase, the gyroid morphology disappears and the hexagonally packed cylindrical morphology becomes dominant. In a higher temperature region where the PE segments are perfectly melted, the morphology changes from the cylindrical to the spherical structure. It is important to notice that the gyroid structure is realized for the state consisting of the molten PEO and the orthorhombic PE and that the cylindrical morphology starts to appear on the way to structural disordering of the PE orthorhombic crystal and shows a maximum when PE parts transform to the rotator phase. In this way the morphological change occurs when the chain aggregation states become thermally unstable by heating. Experimental or theoretical estimation of chain mobility might be helpful for this discussion.

These morphological changes are similar to those detected for the amorphous–crystalline diblock copolymers such as PEO-*b*-PEE^{12,13} and PEO-*b*-PPO.^{14,15} Once the PEO segments are melted, the PE-*b*-PEO block copolymer changes to the crystalline–amorphous diblock copolymer. Therefore, the systematic morphological changes detected in the high temperature region of PE-*b*-PEO diblock copolymer are quite reasonable compared with the behavior of the crystalline–amorphous diblock copolymers. However, it should be emphasized here that we have succeeded in clarifying the relationship between the morphological change and the inner structure change such as orthorhombic-to-hexagonal phase transition on the basis of organizedly combined various kinds of techniques including IR, Raman, WAXD, and SAXS as well as the thermal analysis.

So far, the structural change in mesoscopic level has been treated on the basis of mean field approximation theory,²⁸ but the details of the transition behavior, which are different for the individual diblock copolymer, must be interpreted from the molecular level by taking into account the characteristic features of the copolymer segments. In such a sense, the information obtained in the present study is useful and valuable.

Acknowledgment. This research was made under the financial supported by a MEXT “Collaboration with Local Communities” Project (2005–2009).

References and Notes

- (1) Hamley, I. W. *The Physics of Block Copolymers*; Oxford University Press: New York, 1998.
- (2) (a) Sakurai, S.; Kawada, H.; Hashimoto, T.; Fetters, L. J. *Macromolecules* **1993**, *26*, 5796. (b) Matsen, M. W.; Bates, F. S. *Macromolecules* **1996**, *29*, 1091. (c) Hillmyer, M. A.; Bates, F. S.; Almdal, K.; Mortensen, K.; Ryan, A. J.; Fairclough, J. P. A. *Science* **1996**, *271*, 976. (d) Hasegawa, H.; Hashimoto, T. *Comprehensive Polymer Science*, 2nd Supplement **1996**, 497. (e) Kimishima, K.; Koga, T.; Hashimoto, T. *Macromolecules* **2000**, *33*, 968. (f) Loo, Y.-L.; Register, R. A.; Adamson, D. H.; Ryan, A. J. *Macromolecules* **2001**, *34*, 8968. (g) Hashimoto, T. *Macromol. Symp.* **2001**, *174*, 69. (h) Choi, S.; Vaidya, N. Y.; Han, C. D.; Sota, N.; Hashimoto, T. *Macromolecules* **2003**, *36*, 7707. (i) Park, M. J.; Bang, J.; Harada, T.; Char, K.; Lodge, T. P. *Macromolecules* **2004**, *37*, 9064.
- (3) (a) Rangarajan, P.; Register, R. A.; Fetters, L. J. *Macromolecules* **1993**, *26*, 4640. (b) Rangarajan, P.; Register, R. A.; Adamson, D. H.; Fetters, L. J.; Bras, W.; Naylor, S.; Ryan, A. J. *Macromolecules* **1995**, *28*, 1422.

- (c) Rangarajan, P.; Register, R. A.; Fetters, L. J.; Bras, W.; Naylor, S.; Ryan, A. *J. Macromolecules* **1995**, *28*, 4932. (d) Richter, D.; Schneiders, D.; Monkenbusch, M.; Willner, L.; Fetters, L. J.; Huang, J. S.; Lin, M.; Mortensen, K.; Farago, B. *Macromolecules* **1997**, *30*, 1053. (e) Hamley, I. W. *Adv. Polym. Sci.* **1999**, *148*, 113. (f) Hamley, I. W.; Fairclough, J. P. A.; Ryan, A. J.; Mai, S. M.; Booth, C. *Phys. Chem. Chem. Phys.* **1999**, *1*, 2097. (g) Zhu, L.; Calhoun, B. H.; Ge, Q.; Quirk, R. P.; Cheng, Z.; Thomas, E. L.; Hsiao, B. S.; Yeh, F.; Liu, L.; Lotz, B. *Macromolecules* **2001**, *34*, 1244. (g) Zhu, L.; Cheng, S. Z. D.; Calhoun, B. H.; Ge, Q.; Quirk, R. P.; Thomas, E. L.; Hsiao, B. S.; Yeh, F.; Lotz, B. *Polymer* **2001**, *42*, 5829. (h) Loo, Y. L.; Register, R. A.; Ryan, A. J. *Macromolecules* **2002**, *35*, 2365. (i) Hamley, I. W.; Castelletto, V.; Floudas, G.; Schipper, F. *Macromolecules* **2002**, *35*, 8839.
- (4) (a) Shiomi, T.; Imai, K.; Takenaka, K.; Takeshita, H.; Hayashi, H.; Tezuka, Y. *Polymer* **2001**, *42*, 3233. (b) Fujiwara, T.; Miyamoto, M.; Kimura, Y.; Iwata, T.; Doi, Y. *Macromolecules* **2001**, *34*, 4043. (c) Ho, R.-M.; Hsieh, P.-Y.; Tseng, W.-H.; Lin, C.-C.; Huang, B.-H.; Lotz, B. *Macromolecules* **2003**, *36*, 9085. (d) Nojima, S.; Akutsu, Y.; Akaba, M.; Tanimoto, S. *Polymer* **2005**, *46*, 4060. (e) Takeshita, H.; Fukumoto, K.; Ohnishi, T.; Ohkubo, T.; Miya, M.; Takenaka, K.; Shiomi, T. *Polymer* **2006**, *47*, 8210. (f) Nojima, S.; Kiji, T.; Ohguma, Y. *Macromolecules* **2007**, *40*, 7566. (g) Nojima, S.; Ito, K.; Ikeda, H. *Polymer* **2007**, *48*, 3607.
- (5) Tadokoro, H. *Structure of Crystalline Polymers*; New York: Wiley, 1979.
- (6) (a) Tadokoro, H.; Chatani, Y.; Yoshihara, T.; Tahara, S.; Murahashi, S. *Macromol. Chem.* **1964**, *73*, 109. (b) Takahashi, Y.; Tadokoro, H. *Macromolecules* **1973**, *6*, 672. (c) Takahashi, Y.; Sumita, I.; Tadokoro, H. *J. Polym. Sci., Polym. Phys. Ed.* **1973**, *11*, 2113. (d) Tashiro, K.; Kobayashi, M.; Tadokoro, H. *Rep. Progr. Polym. Phys. Jpn* **1978**, *21*, 417. (e) Shimomura, M.; Tanabe, Y.; Watanabe, Y.; Kobayashi, M. *Polymer* **1990**, *31*, 1411. (f) Masatoki, S.; Matsuura, H. *J. Chem. Soc. Faraday Trans.* **1994**, *90*, 2769. (g) Ding, Y.; Rabolt, J. F.; Chen, Y.; Olson, K. L.; Baker, G. L. *Macromolecules* **2002**, *35*, 3914.
- (7) (a) Hamley, I. W.; Castelletto, V.; Mykhaylyk, O. O.; Yang, Z. *Langmuir* **2004**, *20*, 10785. (b) Marinov, V. S.; Nickolov, Z. S.; Matsuura, H. *J. Phys. Chem.* **2001**, *105*, 9953. (c) Tonegawa, A.; Ohno, K.; Matsuura, H.; Yamada, K.; Okuda, T. *J. Phys. Chem.* **2002**, *106*, 13211.
- (8) Sun, L.; Liu, Y.; Zhu, L.; Hsiao, B. S.; Avila-Orta, C. A. *Polymer* **2004**, *45*, 8181.
- (9) Sun, L.; Liu, Y.; Zhu, L.; Hsiao, B. S.; Avila-Orta, C. A. *Macromol. Rapid Commun.* **2004**, *25*, 853.
- (10) Castillo, R. V.; Arnal, M. L.; Muller, A. J.; Hamley, I. W.; Castelletto, V.; Schmalz, H.; Abetz, V. *Macromolecules* **2008**, *41*, 879.
- (11) Matusura, H.; Fukuhara, K.; Masatoki, S.; Sakakibara, M. *J. Am. Chem. Soc.* **1991**, *113*, 1193.
- (12) Hajduk, D. A.; Kossuth, M. B.; Hillmyer, M. A.; Bates, F. S. *J. Phys. Chem. B* **1998**, *102*, 4269.
- (13) Hamersky, M. W.; Hillmyer, M. A.; Tirrell, M.; Bates, F. S.; Lodge, T. P. *Macromolecules* **1998**, *31*, 5363.
- (14) Alexandridis, P.; Olsson, U.; Lindman, B. *Langmuir* **1996**, *12*, 1419.
- (15) Linse, P. *Macromolecules* **1993**, *26*, 4437.
- (16) Chu, B.; Hsiao, B. S. *Chem. Rev.* **2001**, *101*, 1727.
- (17) Krimm, S.; Liang, C. Y.; Sutherland, G. B. B. M. *J. Chem. Phys.* **1956**, *25*, 549.
- (18) Tasumi, M.; Shimanouchi, T. *J. Chem. Phys.* **1965**, *43*, 1245.
- (19) Tashiro, K.; Sasaki, S.; Kobayashi, M. *Macromolecules* **1996**, *29*, 7460.
- (20) Snyder, R. G.; Maroncelli, M.; Qi, S. P.; Strauss, H. L. *Science* **1981**, *214*, 188.
- (21) Maroncelli, M.; Qi, S. P.; Strauss, H. L.; Snyder, R. G. *J. Am. Chem. Soc.* **1982**, *104*, 6327.
- (22) Kim, Y.; Strauss, H. L.; Snyder, R. G. *J. Phys. Chem.* **1989**, *93*, 7520.
- (23) Strobl, G.; Ewen, B.; Fischer, E. W.; Piesczek, W. *J. Chem. Phys.* **1974**, *61*, 5257.
- (24) Pyckaert, J. P.; McDonald, I. R.; Klein, M. L. *Mol. Phys.* **1989**, *93*, 7520.
- (25) King, H. E., Jr.; Sirota, E. B.; Singer, D. M. *J. Phys. D: Appl. Phys.* **1993**, *26*, B133.
- (26) Sirota, E. B.; King, H. E., Jr.; Singer, D. M.; Shao, H. H. *J. Chem. Phys.* **1995**, *98*, 5809.
- (27) Hamley, I. W.; Castelletto, C. *Prog. Polym. Sci.* **2004**, *29*, 909.
- (28) Fredrickson, G. H.; Ganesan, V.; Drolet, F. *Macromolecules* **2002**, *35*, 16.
- (29) Morishita, H.; Kobayashi, M.; Sato, K.; Kondo, H.; Suharto, M. *Nagasaki Daigaku Kyoikugakubu Shizen Kagaku Kenkyu Hokoku* **1995**, *52*, 13.

JP8092435